Electrocatalysis (2019) 10:392–398
https://doi.org/10.1007/s12678-019-00523-8

ORIGINAL RESEARCH

Electrochemical Properties of Polyoxometalate ($H3PMo_{12}O_{40}$) -Functionalized Graphitic Carbon Nitride (g-C_3N_4)

Natasha Ross[1] · Noniko Nqakala[1] · Shane Willenberg[1] · Sabelo Sifuba[1] · Emmanuel Iwuoha[1]

Published online: 4 April 2019

Abstract

A functionalized polyoxometalate/graphitic carbon nitride (PMo_{12}/g-C_3N_4) composite has been constructed to promote direct electron and ion exchange based on a facile, rapid wetness incipient method. The PMo_{12} displayed a natural affinity towards the carbon support which facilitated enhanced reversible redox processes with surface-controlled electron diffusion. The g-C_3N_4-functionalized PMo_{12} composite promoted effective oxidation and reduction of the Keggin molecule addenda atoms with reduced overpotential without the mediation of a polymeric linker to promote their exposure and interaction. The g-C_3N_4 offered increased surface area for anchoring PMo_{12}, structural stability at increased temperatures, and repeated cycling as well as control of the density and position of PMo_{12} as probed by scanning electron microscopy and nuclear magnetic resonance spectroscopy, respectively. These results demonstrate that PMo_{12} clusters are sensitive to their local environment, including the interaction with the support, which stimulated enhanced current mobility.

Keywords Electrochemistry · Composite · Electron diffusion · g-C_3N_4 · Polyoxometalates

Introduction

Over the last decade, polyoxometalates ($H_3PMo_{12}O_{40}$) have enthused many research activities over a broad spectrum of science, such as catalysis, materials, and medicine, because of their chemical properties such as redox potential, acidity, and solubility in various media [1, 2]. The PMo_{12} belongs to a large family of heteropolyanions with the so-called Keggin structure, where a tetrahedral XO_4 core (X = P in this case) serves as a template for the aggregation of 12 MoO_6 octahedral sharing corners and edges. Keggin-type polyoxometalates are capable of multiple redox reactions which make them particularly useful for electrochemistry [3]. Their hierarchical crystal structure however greatly influences the accessibility of their active sites and the location of the protons [4, 5]. Owing to this unique cluster structure, PMo_{12} has very low surface area with negligible conductivity. Therefore, in order to maximize electron transfer kinetics, ideally each PMo_{12} cluster molecule should be electrically linked to a conductive substrate [6, 7]. According to the literature, PMo_{12} anchored to carbon-based materials in particular promotes multielectron reversible redox reactions. This allows each cluster anion to engage in electrochemistry and as such provide the greatest active surface for interaction with the electrolyte. Graphene in particular has been reported as a good support material due to its large surface area and high electrical conductivity. The difficulties related to the integration between PMo_{12} and graphene as well as effective control of the density and position of PMo_{12}, however, are alleviated through an organic linker used to bridge the two components enabling contact and charge transfer at the interface [8, 9]. As a novel function material, graphitic carbon nitride is regarded as an ideal support matrix because of its exceptionally high surface area and the prospect of monolayer coverages even at high PMo_{12} loading. Concomitantly, g-C_3N_4 exhibits a unique stability, heat endurance, and chemical resistance to intimately bond PMo_{12} [10, 11]. In addition, the presence of nitrogen in g-C_3N_4 itself plays an important role in improving the wettability of the electrode with the electrolytes and concomitantly promotes electrochemical interactions [12, 13].

In this study, the aptitude of the mesoporous g-C_3N_4 to firmly anchor bulky PMo_{12} electroactive inorganic anions

✉ Natasha Ross
nross@uwc.ac.za

[1] SensorLab, Department of Chemistry, University of the Western Cape, Private Bag X17, Bellville, Cape Town 7535, South Africa

to facilitate enhanced redox activity and stability under catalytic conditions in the absence of an organic linker was explored. The morphology, electronic structure, and synergy of the composite materials towards exposing PMo_{12} active sites for improved interactions were probed by advanced spectroscopic, microscopic, and electrochemical techniques. The positive stimulus of the PMo_{12}/g-C_3N_4 was validated by enhanced redox properties. The area under the current-voltage curve for PMo_{12}/g-C_3N_4 was indicative of enhanced capacitive performance and increased electron density on the PMo_{12} anion and reducibility.

Experimental

The mesoporous graphitic carbon nitride, g-C_3N_4, was synthesized using a method previously developed with minor adjustments [14, 15]. In a typical procedure, 3.0 g dicyandiamide was added to 50 mL of an aqueous solution containing Triton X-100 at 60 °C under magnetic stirring. After evaporation, the resultant solid was dried in an air oven at 60 °C overnight, followed by heating to 550 °C at a heating rate of 5 °C min^{-1} in N_2 and kept there for 4 h. Phosphomolybdic acid hydrate ($PMo_{12}O_{40}{\cdot}xH_2O$) was obtained from Fischer Scientific. The synthesis of the PMo_{12}/g-C_3N_4 composite was accomplished by a simple wetness incipient method [16]. In a typical procedure, the concentration of the PMo_{12} solution was adjusted to obtain 24% of the theoretical maximum surface coverage, corresponding to 10 wt%. The required volume of the solutions was slowly added to the g-C_3N_4 support (under vigorous magnetic stirring). After water evaporation, the resultant solid was dried at 100 °C, and then calcined at 350 °C for 2 h with a heating rate of 5 °C min^{-1} to obtain a desired composite. The obtained sample was denoted PMo_{12}/g-C_3N_4. The morphology, composition, and particle size were probed by scanning electron microscopy (SEM, Zeiss Neon 40EsB FIBSEM). The PMo_{12}/g-C_3N_4 local environment and stability with increased temperature were probed by ^{31}P NMR analysis (Bruker, Advance 400 WB, DSX-400). The cyclic voltammetry (CV) and electrochemical impedance spectroscopy (EIS) measurements were recorded on a multichannel potentiostat (Bio-Logic VMP2) in order to further probe any changes in the electronic structure of PMo_{12} clusters that resulted from their dispersion and electronic interaction with g-C_3N_4. X-ray photoelectron spectroscopy (XPS) was performed to measure the elemental composition, chemical state, and electronic state of the elements that exist within a material. This was done on an ultrahigh vacuum VG ESCALAB 210 electron spectrometer with Mg Kα radiation ($h\nu$ = 1253.6 eV). The binding energy was referenced to the C1s peak at 283.8 eV of the surface-exposed adventitious carbon.

Results and Discussion

Structural Characterization

The hollow to cloud-like morphology of the g-C_3N_4 surface is evident of its isotropic structure as shown by the SEM image in Fig. 1a. The PMo_{12} distribution is primarily controlled by the g-C_3N_4 platform architecture. After functionalization by $PMo_{12,}$ the PMo_{12}/g-C_3N_4 composite shows a more complex surface morphology as illustrated in Fig. 1b. The PMo_{12} distributed all over the g-C_3N_4 substrate corresponded to a high surface coverage as shown at higher magnification in Fig. 1c. The energy dispersive spectroscopy (EDS) map and spectrum confirm (Fig. 1d, f) the presence of both g-C_3N_4 and PMo_{12} by the wide-ranging distribution and of the C, Mo, P, O, and N elements. Higher phosphorus composition corresponds to areas with a higher density of PMo_{12} clusters. The overall unique ternary structure provides more electrochemically active sites for electrolyte exposure [17, 18], stimulating ion transfer which promotes the surface redox reactions and conductance as corroborated by CV and EIS.

The phase, purity, molecular structure, and thermal stability of PMo_{12}/g-C_3N_4 were probed by solid-state ^{31}P MAS NMR analysis. The spectrum of PMo_{12}/g-C_3N_4 compared with that of unsupported PMO_{12} is shown in Fig. 2. The number of ^{31}P peaks for PMo_{12}, shown in Fig. 2 a, corresponds to the existence of one intense PMo_{12} anhydrous phase and one less intense broader amorphous phase signal being in good agreement with the literature [19, 20]. After modification, the anhydrous phase peak moves downfield, i.e., the nuclei become less shielded, whereas the amorphous phase signal moves upfield, i.e., the nuclei become less shielded. This phenomenon and the small charge changes of oxygen atoms occur in the oxygen vacancy formation for the PMo_{12} signal; the presence of additional ^{31}P MAS signals indicates a higher stability of supported PMo_{12}, compared with that of the bulk material. Therefore, the downfield shift of ^{31}P NMR is assigned to PMo_{12} crystallites with a different number of water molecules lost during impregnation, but the phases are well-resolved due to chemical interaction with the g-C_3N_4 [21]. It can be concluded that the primary structure (Keggin unit) is preserved after attachment to g-C_3N_4. This amorphous phase also shows to be affected by change in temperature as shown in Fig. 2 b. The peak becomes broader and less intense as temperature increases from 25 to 50 °C, which signals the formation of an anhydrous structure. The thermal resistance of this phase is higher

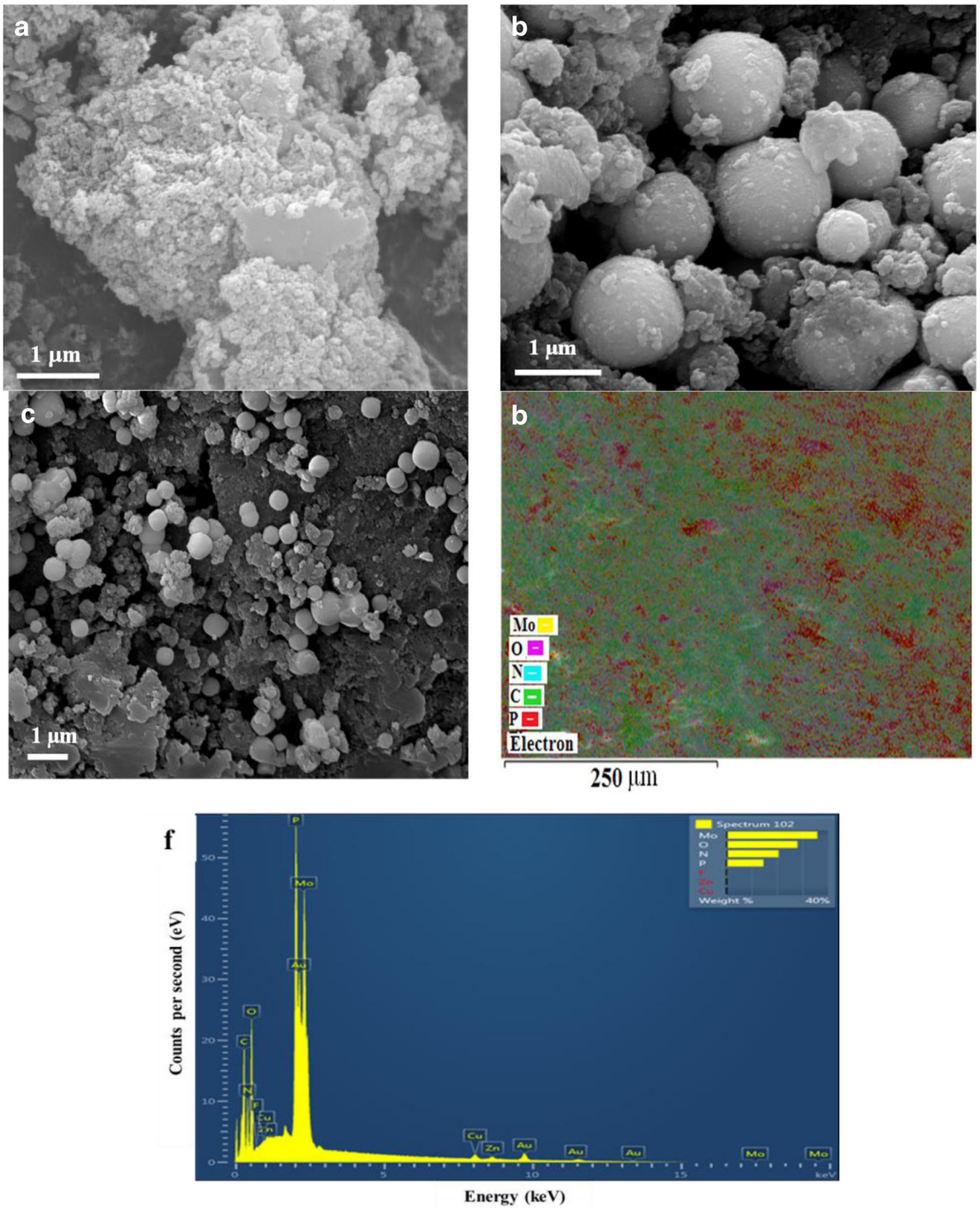

Fig. 1 High-resolution SEM images of **a** mesoporous g-C_3N_4, **b** PMo_{12}/g-C_3N_4, and **c** a section of b enlarged. **d** 2D elemental map of the composite with corresponding **f** EDS spectrum

due to the interaction between the PMo_{12} anion and g-C_3N_4. Therefore, the Keggin structure is thermally stable in the studied temperature range. These conclusions coincide with PMo_{12} supported on TiO_2 [22].

The deconvoluted Mo 3d, P 2p, C1s, N1s and O1s spectra of PMo_{12}/g-C_3N_4 are shown in Fig. 3. The high-resolution Mo 3d spectrum displays two peaks at binding energies of 232.8 eV and 236.0 eV, corresponding to the Mo $3d_{3/2}$ and Mo $3d_{5/2}$ spin-orbit states of PMo_{12}, respectively [23]. The C1s XPS spectrum of the composite shows two kinds of carbon atoms in different functional groups: C–C/C=C bonds (283.9 eV) and C–O bands (286.8 eV). The N1s spectrum consists of four main contributions. The two main signals at 398.6 eV and 400.4 eV correspond to

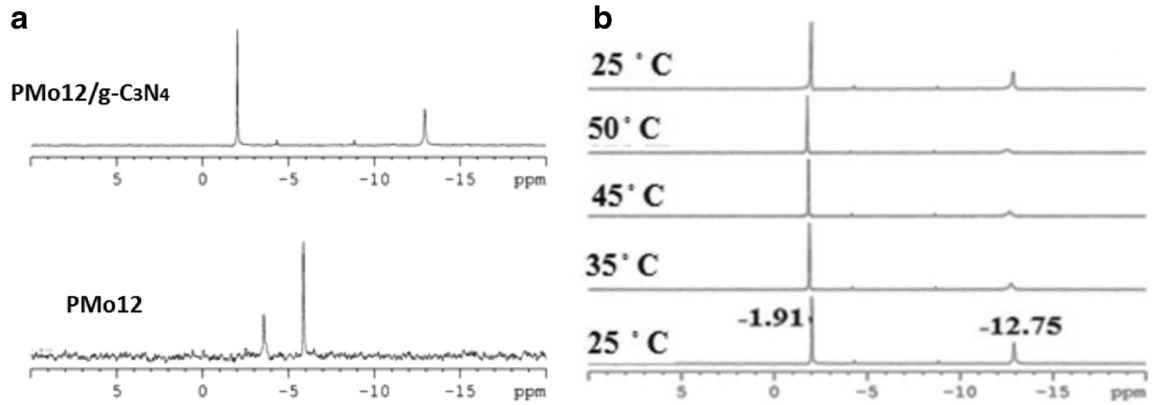

Fig. 2 $^{31}P\{1H\}$ NMR spectra of **a** PMo_{12} and $PMo_{12}/g\text{-}C_3N_4$ with a corresponding **b** temperature study

two types of sp2 hybridized nitrogen: Nα (bonded to two adjacent atoms) and Nβ (bonded to three bordering atoms), respectively, which agrees with the recent work done by Zhu et al. [24]. The position of the O1s signals is located at 529.8 eV and another wider peak positioned at 531.6 eV, which verifies the successful attachment of PMo_{12} species.

Electrochemical Characterization

Electrochemical measurements (CV and EIS) were conducted to probe the redox activity of PMo_{12} resulting from their direct dispersion and chemical interaction with g-C_3N_4. The electrochemistry of g-C_3N_4, pure PMo_{12}, and functionalized g-C_3N_4 modified on glassy carbon electrode (GCE) in 0.5 M H_2SO_4 solution is presented in Fig. 4a–c, respectively. The Nyquist plots of PMo_{12} and PMo_{12}/C_3N_4 are shown in Fig.4 d.

The redox activities of the different modified electrodes were studied in a conventional three-electrode system in 0.5 M H_2SO_4 electrolyte solutions. As illustrated in Fig. 4 a, the CV exhibits three-step redox waves of PMo_{12} denoted by i, ii, and iii, with the midpoint potentials E_{mid} of 0.35, 0.2, and − 0.07 V, respectively. The PMo_{12} was not stable during the measurement due to progressive leaching into the electrolyte, as demonstrated by the decreasing amplitude of the peaks with sequential scans. The g-C_3N_4 (Fig. 4 b) showed no observable redox peaks within the voltage window, which is attributed to the weak electrical conductivity of g-C_3N_4 and the absence of adsorbed redox species on the surface. Reversible redox peaks are observed for 10% $PMo_{12}/g\text{-}C_3N_4$/GCE, originating from the stabilized PMo_{12} and successful chemical interactions which promote charge diffusion. The current response increased with the increase of the scan rate (Fig. 4c), and similar curves with three pairs of redox peaks were observed at all scan rates, with no obvious distortion [25]. This observation indicates sufficient electron transfer from the PMo_{12} cluster to the electrode in all subsequent redox steps. The shift to lower reduction potentials indicates that the $PMo_{12}/g\text{-}C_3N_4$ composite has increased electron density on the polyoxometalate (POM) anion and reducibility. Concomitantly, no leaching was observed when the potential was cycled between − 0.2 and 0.5 V. Based on the redox peaks of $PMo_{12}/g\text{-}C_3N_4$, their peak separations (ΔE_p) were calculated to be as small as ≈ 23–26 mV. This allows for the surface coverage to be estimated by the equation for reversible surface-confined species according to the equation: Peak current is directly proportional to surface coverage (Γ) and scan rate (ν). From Eq. 1, there is a linear relationship between i_p (and the current at any one point on the voltammetric curve) and ν, facilitating as a useful indicator of a surface-confined species.

$$i_p = \frac{n^2 F^2 \Gamma A \upsilon}{4RT} \tag{1}$$

Since the peak separation is small, the surface coverage can be estimated approximately from cyclic voltammetry by the Eq. 2 for reversible surface-confined species as follows:

$$\Gamma = \frac{4 i_{pa} RT}{n^2 F^2 \nu A} \tag{2}$$

where n is the number of electrons transferred, ν is the scan rate (V/s), A is the geometric area of the electrode (0.0725 cm^2), Γ is the surface coverage of the electroactive species, R is the gas constant, T is the temperature (298 K), and F is the Faraday constant. This led to a value of 1.2×10^9 mol cm^2 for $PMo_{12}/g\text{-}C_3N_4$, which corresponds to around 0.66 monolayer coverage. This agrees favorably with the work done by Choi and Kim, based on functionalized Keggin-type polyoxometalates [26]. From EIS results shown in Fig. 4 d, the semicircle radius on the Nyquist plot for PMo_{12}/C_3N_4 is much smaller than that for PMo_{12}, clearly confirming the PMo_{12}/C_3N_4 to have improved charge transfer. Concomitantly, the conductance of 52.9 μF for pure PMo_{12} and 79.5 μF for PMo_{12}/C_3N_4 indicates that the supported PMo_{12} has enhanced redox activity. The g-C_3N_4 allowed for the large inorganic heteropolyanions to remain anchored and exhibit improved conductive behavior. Even in the absence of

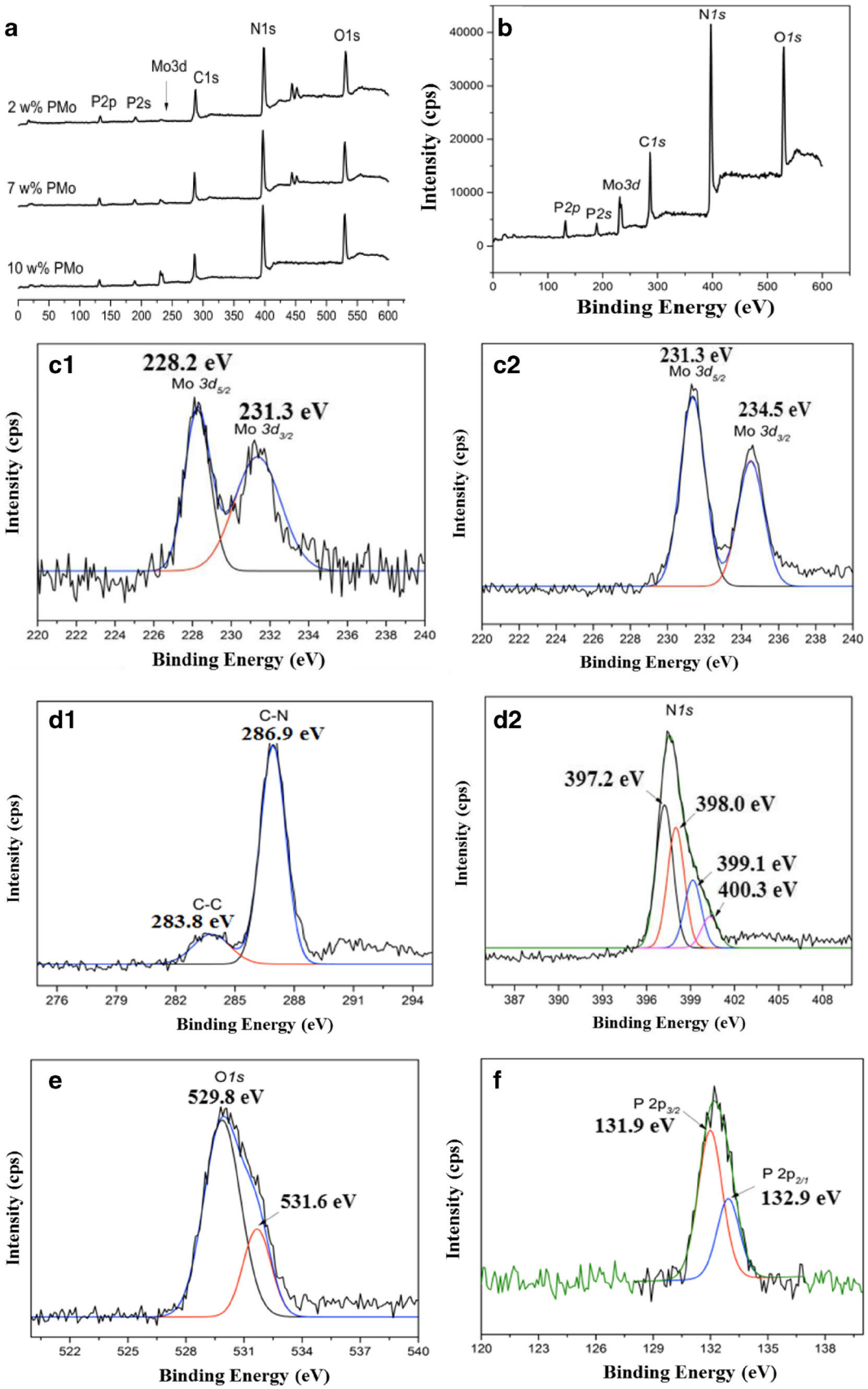

Fig. 3 XPS spectra. **a**, **b** Full scan of the PMo_{12}/g-C_3N_4 composite. Deconvoluted XPS spectra of **c1**, **2** Mo 3d; **d1**, **2** C1s and N1s; **e** O1s; and **f** P 2p

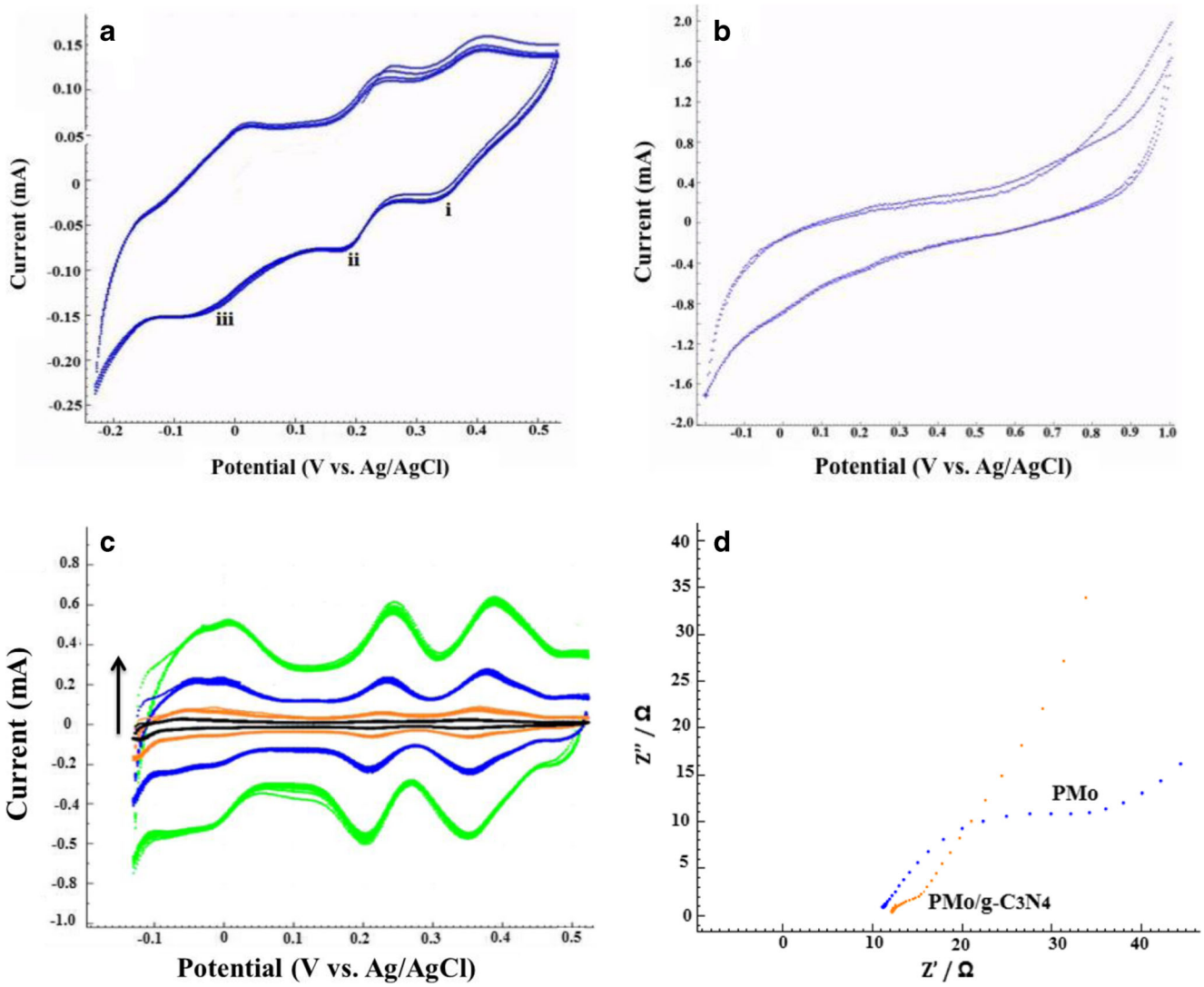

Fig. 4 CV of **a** pure PMo_{12}/GCE at 50 mV/s, **b** g-C_3N_4/GCE at 50 mV/s, and **c** 10% PMo_{12}/C_3N_4/GCE at 5–50 mV/s in 0.5 M H_2SO_4. **d** Nyquist plots of PMo_{12}/GCE and 10% PMo_{12}/C_3N_4/GCE at 50 mV

a positively charged linker (usually applied to provide good interaction), the direct synergy between PMo_{12}/C_3N_4 improved the accessibility of the POM active sites, improved the redox performance, and demonstrated stable amplitude upon repeated scanning. These results, in addition to structural stability, are important factors contributing to the efficiency of cation insertion electrodes [27–30].

Conclusions

We have accomplished the chemical synthesis of a hybrid material based on PMo_{12} successfully attached to g-C_3N_4 as support; the POMs functioned as electron storage sites, as well as electron transfer mediators. The high surface area of the g-C_3N_4 allowed a high dispersion of PMo_{12} down to the molecular level. Spectroscopic and electrochemical investigations revealed that the structure and the electronic properties of the PMo_{12} are improved as a result of the synergy with the graphitic carbon nitride (g-C_3N_4). The preparation of PMo_{12}/g-C_3N_4 was simple to perform, leading to reproducible and stable electrode material. The results show how the local chemical environment influences the electron transfer activity of PMo_{12}. Disseminated PMo_{12}, anchored on g-C_3N_4 as electrocatalytically active sites, contributes towards higher interfacial charge transfer and proves feasible as active electrode material in technological electrochemical devices.

Funding Information This paper was financially supported by South Africa's National Research Foundation (NRF).

Compliance with Ethical Standards

Competing Interests The authors declare that they have no competing interests.

References

1. Y. Ji, L. Huang, J. Hu, C. Streb, Y.-F. Song, Polyoxometalate-functionalized nanocarbon materials for energy conversion, energy storage and sensor systems. Energy Environ. Sci. **8**(3), 776–789 (2015)
2. K. Kamata, K. Sugahara, Base catalysis by mono- and polyoxometalates. Catalysts. **7**(11), 345 (2017)
3. S.S. Wang, G.Y. Yang, Recent advances in polyoxometalate-catalyzed reactions. Chem.Rev. **115**(11), 4893–4962 (2015)
4. M.T.A. Pope, *Introduction to Polyoxometalate Chemistry, Polyoxometalate Molecular Science*, vol 98 (Springer, Dordrecht, 2003), pp. 3–31
5. M. Sadakane, E. Steckhan, Electrochemical properties of polyoxometalates as electrocatalysts. Chem. Rev. **98**(1), 219–237 (1998)
6. R. Tsunashima, Y. Iwamoto, Y. Baba, C. Kato, K. Ichihashi, S. Nishihara, K. Inoue, K. Ishiguro, Y.-F. Song, T. Akutagawa, Electrical network of single-crystalline metal oxide nanoclusters wired by π-molecules. Angew. Chem. Int. **54**, 11228–11231 (2014)
7. M. Genovese, Y.W. Foong, K. Lian, Designing polyoxometalate based layer-by-layer thin films on carbon nanomaterials for pseudocapacitive electrodes. J. Electrochem. Soc. **162**(5), A5041–A5046 (2015)
8. H. Li, S. Pang, S. Wu, X. Feng, K. Muller, C. Bukbeck, Layer-by-layer assembly and UV photoreduction of graphene-polyoxometalate composite films for electronics. J. Am. Chem. Soc. **133**(24), 9423–9429 (2011)
9. Z. Shuang-Shuang, L. Rong-Ji, Z. Guang-Jin, G. Zhan-Jun, Functionalization of carbon nanotubes/graphene by polyoxometalates and their enhanced photo-electrical catalysis. Chin. Phys. B **23**, 088801 (2014)
10. Y. Fu, J. Zhu, C. Hu, X. Wu, X. Wang, Covalently coupled hybrid of graphitic carbon nitride with reduced graphene oxide as a superior performance lithium-ion battery anode. Nanoscale. **21**, 12555–12564 (2014)
11. S.A. Ansari, M.H. Cho, Simple and large scale construction of MoS_2-g-C_3N_4 heterostructures using mechanochemistry for high performance electrochemical supercapacitor and visible light photocatalytic applications. Sci. Rep. **7**(1), 43055 (2017)
12. N. Casan-Pastor, P. Gomez-Romero, Polyoxometalates: from inorganic chemistry to materials science. Front. Biosci. **9**(1-3), 1759–1770 (2004)
13. L. Shi, J. Zhang, H. Liu, M. Que, X. Cai, S. Tan, L. Huang, Flower-like $Ni(OH)_2$ hybridized g-C_3N_4 for high-performance supercapacitor electrode material. Mater. Lett. **145**, 150–153 (2015)
14. J. Liu, H. Wang, M. Antonietti, Graphitic carbon nitride "reloaded": emerging applications beyond (photo) catalysis. Chem. Soc. Rev. **45**(8), 2308–2326 (2016)
15. H. Gong, J. Zhu, K. Lv, P. Xiao, Y. Zhao, Templating synthesis of metal oxides by an incipient wetness impregnation route and their activities for CO oxidation. New J. Chem. **39**(12), 9380–9388 (2015)
16. H. Yanga, K. Lva, J. Zhua, Q. Li, D. Tanga, W. Hoc, M. Li, Carabineirod, effect of mesoporous g-C3N4 substrate on catalytic oxidation of CO over Co_3O_4. Appl. Surf. Sci. **401**, 333–340 (2017)
17. Y. Li, P.K. Shen, Simultaneous formation of ultrahigh surface area and three-dimensional hierarchical porous graphene-like networks for fast and highly stable supercapacitors. Adv. Mater. **25**(17), 2474–2480 (2013)
18. H. Sun, X. You, J. Deng, X. Chen, Z. Yang, J. Ren, H. Peng, Novel graphene/carbon nanotube composite fibers for efficient wire-shaped miniature energy devices. Adv. Mater. **26**(18), 2868–2873 (2014a)
19. C. Shi, R. Wang, G. Zhu, S. Qiu, J. Long, Synthesis, characterization, and catalytic properties of SiPW-X mesoporous silica with heteropolyacid encapsulated into their framework, synthesis. Eur. J. Inorg. Chem. **23**, 4801–4807 (2005)
20. A.L. Skinner, J.S. Laurence, High-field solution NMR spectroscopy as a tool for assessing protein interactions with small molecule ligands. J. Pharm. Sci. **97**(11), 4670–4695 (2008)
21. S. Ganapathy, M. Fournier, J.F. Paul, L. Delevoye, M. Guelton, J.P. Amoureux, Location of protons in anhydrous Keggin heteropolyacids H(3)PMo12(12)O(40) and H(3)PW(12)O(40) by (1)H[(31)P]/(31)P[(1)H] REDOR NMR and DFT quantum chemical calculations. J. Am. Chem. Soc. **26**, 7821–7828 (2002)
22. S. Damyanova, J.L.G. Fierro, Structural features and thermal stability of titania-supported 12-molybdophosphoric heteropoly compounds. Chem. Mater. **10**(**3**), 871–879 (1998)
23. M. Sun, Y. Wang, Y. Shao, Y. He, Q. Zeng, H. Liang, T. Yan, B. Du, Fabrication of a novel Z-scheme g-C_3N_4/Bi_4O_7 heterojunction photocatalyst with enhanced visible light-driven activity toward organic pollutants. J. Colloid Interface Sci. **501**, 123–132 (2017)
24. B. Zhu, P. Xia, Y. Li, W. Ho, J. Yu, Fabrication and photocatalytic activity enhanced mechanism of direct Z-scheme g-C_3N_4/Ag_2WO_4 photocatalyst. Appl. Surf. Sci. **391**, 175–183 (2017)
25. K.K. Kasem, F.A. Schultz, Electrochemistry of polyoxometalates immobilized in ion exchange polymer films. J. Inorg. Organomet. Polym. **4**(4), 377–390 (1994)
26. S. Choi, J. Kim, Adsorption properties of Keggin-type polyoxometalates on carbon based electrode surfaces and their electrocatalytic activities. Bull. Kor. Chem. Soc. **30**, 810–816 (2009)
27. S. Herrmann, C. Ritchie, C. Streb, Polyoxometalate–conductive polymer composites for energy conversion, energy storage and nanostructured sensors, Royal Society of Chemistry. Dalton Trans **44**, 7092–7104 (2015)
28. S. Gupta, B. Aberg, S.B. Carrizosa, Functionalized graphene–polyoxometalate nanodots assembly as "organic–inorganic" hybrid supercapacitors and insights into electrode/electrolyte interfacial processes. C-Journal of Carbon Research **3**(4), 24 (2017)
29. T. Wei, M. Zhang, P. Wu, Y.-Q. Lan, POM-based metal-organic framework/reduced graphene oxide nanocomposites with hybrid behavior of battery-supercapacitor for superior lithium storage. Nano Energy **34**, 205–214 (2017). https://doi.org/10.1016/j.nanoen.2017.02.028
30. W. Ong, L.L. Tan, Y. Ng, S. Yong, S. Chai, Graphitic carbon nitride (g-C_3N_4)-based photocatalysts for artificial photosynthesis and environmental remediation: are we a step closer to achieving sustainability? Chem. Rev. **116**(12), 7159–7329 (2016)